

1 Resilience Pathways for Halide Perovskite Photovoltaics Under Temperature Cycling

2 Luyan Wu (吴录艳)^{1,2†}, Shuaifeng Hu (胡帅锋)^{3†}, Feng Yang (杨枫)^{4,5†}, Guixiang Li (李桂香)^{1,6*},
3 Junke Wang (王竣可)³, Weiwei Zuo (左巍巍)⁷, José J. Jerónimo-Rendon⁷, Silver-Hamill Turren-
4 Cruz⁸, Michele Saba², Michael Saliba^{7,9}, Mohammad Khaja Nazeeruddin⁶, Jorge Pascual^{10*}, Meng Li
5 (李萌)^{4*}, Antonio Abate^{1,11*}

6 ¹Helmholtz-Zentrum Berlin für Materialien und Energie GmbH, Hahn-Meitner-Platz 1, 14109 Berlin,
7 Germany.

8 ²Department of Physics, Università degli Studi di Cagliari, Monserrato (CA), I-09042, Italy.

9 ³Clarendon Laboratory, Department of Physics, University of Oxford, Oxford OX1 3PU, U.K.

10 ⁴Key Lab for Special Functional Materials of Ministry of Education, National & Local Joint
11 Engineering Research Center for High-efficiency Display and Lighting Technology, School of
12 Nanoscience and Materials Engineering, and Collaborative Innovation Center of Nano Functional
13 Materials and Applications, Henan University, Kaifeng 475004, P. R. China.

14 ⁵College of Physics, Henan Key Laboratory of Advanced Semiconductor & Functional Device
15 Integration, Henan Normal University, Xinxiang 453007, China.

16 ⁶Institute of Chemical Sciences and Engineering, École Polytechnique Fédérale de Lausanne (EPFL),
17 1015 Lausanne, Switzerland.

18 ⁷Institute for Photovoltaics (ipv), University of Stuttgart, Pfaffenwaldring 47, D-70569 Stuttgart,
19 Germany.

20 ⁸Instituto de Ciencia de los Materiales (ICMUV), Universidad de Valencia, C/Catedrático José
21 Beltrán 2, E-46980 Paterna, Spain.

22 ⁹Helmholtz Young Investigator Group FRONTRUNNER, IEK5-Photovoltaics Forschungszentrum
23 Jülich 52425 Jülich, Germany.

24 ¹⁰Polymat, University of the Basque Country UPV/EHU, 20018 Donostia-San Sebastian, Spain.

25 ¹¹Department of Chemistry, Bielefeld University, Universitätsstraße 25, 33615 Bielefeld, Germany

26 † These authors contributed equally: L. Wu, S. Hu and F. Yang

27 * Corresponding authors. E-mail: guixiang.li.gl@gmail.com (G. Li), jpascual1992@gmail.com (J.
28 Pascual), mengli@henu.edu.cn (M. Li), antonio.abate@helmholtz-berlin.de (A. Abate)

29

30 Abstract

31 Metal-halide perovskite solar cells have achieved power conversion efficiencies comparable to those
32 of silicon photovoltaic devices, approaching 27% for single-junction devices. The durability of the
33 devices, however, lags far behind their performance. Their practical implementation implies the
34 subjection of the material and devices to temperature cycles of varying intensity due to diurnal cycles
35 or geographical characteristics. Thus, it is vital to develop devices that are resilient to temperature
36 cycling. This Perspective analyses the behavior of perovskite devices under temperature cycling. We
37 discuss the crystallographic structural evolution of the perovskite layer, reactions and/or interactions
38 between stacked layers, photovoltaic properties, and photocatalysed thermal reactions. We highlight
39 effective strategies for improving stability under temperature cycling, such as improving material
40 crystallinity or relieving interlayer thermal stress using buffer layers. Additionally, we outline existing
41 standards and protocols for temperature cycling testing and we propose a unified approach that could
42 facilitate valuable cross-study comparisons among scientific and industrial research labs. Finally, we
43 share our outlook on strategies to develop perovskite photovoltaic devices with exceptional real-world
44 operating stability.

45 **ToC blurb: Device resilience under temperature cycling is critical for the practical**
46 **implementation of perovskite photovoltaics. This perspective highlights how the stability evolves**
47 **with thermal cycling, emphasizing the need for adequate protocols and a deeper understands of**
48 **the materials and interfaces changes.**

49

50 [H1] Introduction

51 Since their early introduction, metal-halide perovskite solar cells (PSCs) have rapidly developed
52 owing to their exceptional photovoltaic (PV) properties¹⁻⁶ and low-cost solution- and vacuum-based
53 fabrication⁷⁻¹⁰. The leading power conversion efficiencies (PCE) of single-junction PSCs now
54 approach 27%^{11,12} and is on par with that of silicon cells. In tandem PVs, double-junction devices with
55 two stacked photo absorbers in series could achieve a potential PCE exceeding 45%¹³, benefiting from
56 the reduced thermalisation loss of the excitons. Thanks to the bandgap tunability¹⁴ and ultra-long
57 carrier diffusion length¹⁵ of metal halide perovskites, depositing, for instance, a 1 μm thick layer of
58 perovskite with a bandgap of ~ 1.7 eV atop a conventional silicon subcell (~ 1.1 eV) enables PCE of
59 over 34% in lab scale small cells and of over 30% in commercial wafer-scale devices. Moreover,
60 monolithic double-junction “all-perovskite” tandems have achieved PCE values of over 30%¹⁶. In
61 principle, multi-junction perovskite-based tandems could reach PCE values of over 50%, constituting
62 the most cost-effective PV products on the market¹³. Efficiency is thus the main asset of PSCs, taking
63 these semiconductors a step closer to practical implementations.

64 The stability of perovskite-based materials and devices, mostly regarding defect generation, ion
65 migration, phase transition and interface degradation, brings up important concerns regarding their
66 future practical potential. To date, studies on perovskite device stability have primarily focused on
67 operational stability at room temperature^{17,18} or on accelerated ageing^{19,20} (for example, under elevated
68 fixed temperature such as +85 °C) to extrapolate the “potential long-term lifespan”²¹⁻³¹. However,
69 during practical operation, PV devices are constantly exposed to temperature changes. Thus, to
70 accurately predict the stability of perovskite PV devices under practical operation³², they need to be
71 studied under temperature cycling, which is a condition that is scarcely explored. Variations in
72 temperature have a critical influence on the structural and chemical changes of the materials, the
73 device structure, and the PV performance, which is different from the exposition to fixed
74 temperatures. Thus, understanding the impact of temperature and temperature cycles on materials and
75 devices, and performing the corresponding stability analysis, is of utmost importance for developing
76 long-term stable perovskite PV technology.

77 The temperature fluctuates with diurnal cycles, seasonal variations, altitude differences, and diverse
78 geographical locations (from the poles to the equator)³³. For instance, extreme temperature changes,
79 for example in deserts, pose additional challenges for the implementation of perovskite PVs³⁴⁻³⁸. Other
80 applications, such as extra-terrestrial use (for example in spacecraft, high-altitude pseudo-satellites,
81 international space stations, and Mars rovers)^{36,39-42}, impose even more severe conditions due to a
82 larger temperature range^{32,43,44}. These temperature cycles have a substantial impact on the lifespan of
83 PV devices⁴⁵⁻⁴⁷, influencing properties such as lattice strain, crystallographic site defects, phase

84 transitions, ion migration, and material diffusion between and among the stacked device layers⁴⁸⁻⁵².
85 Together with the influence of photons and other stressors, temperature cycles could lead to
86 accelerated device failure compared to the commonly employed elevated constant temperature^{19,53-55},
87 and are more representative of the practical outdoor behavior of the devices⁵⁶. Thus, summarizing and
88 understanding the working and failure mechanisms of perovskites and their devices under thermal
89 cycling is particularly meaningful for the development of commercial perovskite-containing PVs.

90 In this Perspective, we discuss the importance of temperature cycling when evaluating long-term
91 perovskite PV stability. We aim to emphasise the temperature-variation-induced degradation of PSCs,
92 which is often disregarded in comparison to degradation at elevated temperatures. We present a
93 systematic overview of the structure and performance evolution of perovskite-based PV devices under
94 temperature cycles, and we compare perovskite materials of different bandgaps to highlight the
95 influence of perovskite composition on temperature-variation-induced degradation. We also propose
96 strategies to improve operational stability under temperature cycling, and we recommend suitable
97 protocols for assessing device evolution under extended thermal cycling. Lastly, we share our
98 opinions on the future challenges for developing perovskite PV devices resistant to temperature
99 cycles.

100

101 **[H1] Impacts of temperature cycling on perovskite photovoltaic devices**

102 Temperature cycling has different impacts on perovskite materials and PV devices. In the perovskite
103 device stack, the layers most affected by temperature cycling are the perovskite layer and the charge
104 transporting layers (CTLs). In the perovskite layer, phase transitions are temperature-dependent and
105 are strongly influenced by perovskite composition. Temperature cycling might lead to irreversible
106 phase transitions and lattice distortions due to strain (**Fig. 1**). In addition, temperature cycling
107 promotes the interaction, diffusion and penetration of perovskite components with the CTLs and its
108 interfaces. Furthermore, dynamic fluctuations in CTLs due to temperature can exert additional strain
109 on the perovskite layer. Finally, temperature has a direct effect on PV parameters. Although the
110 influence of temperature on PV parameters is usually reversible, consecutive cycling can induce a
111 permanent declining trend in the performance.

112 **[H2] Impact on the perovskite layer**

113 Temperature cycling has two main consequences in the integrity of the perovskite layer. First,
114 perovskite crystalline phase is dependent on the environment temperature, therefore consecutive
115 cycles of temperature will impose successive phase transitions that can lead to irreversible
116 degradation. Second, temperature-driven lattice distortions introduce lattice strain in the films that
117 will accumulate with increased cycling.

118 [H3] Phase transitions

119 Temperature drives perovskite phase changes by affecting thermal energy, atomic vibration, and ionic
120 migration (**Fig. 2a**). In general, under thermal cycling, two distinct phase transition behaviors impact
121 the performance of the device.⁵⁷ The first is a reversible phase transition between the cubic and
122 tetragonal phases, which accounts for properties variation within a single thermal cycle. The second is
123 an irreversible phase transition, such as the transformation to the hexagonal photoinactive polytype
124 phase (that is, 4H and 6H)⁵⁸ and decomposition to PbI_2 , which results in continued and unrecoverable
125 degradation of the perovskite and device (**Fig. 2b**). The tetragonal phase (β -phase) is usually retained
126 in the low-temperature region after multiple thermal cycles^{57,59}. Phase transitions are more readily
127 reversible in the out-of-plane direction compared to the in-plane direction where additional forces are
128 exerted by substrate. Under such reversible behavior, device performance is unlikely to experience
129 significant degradation when the temperature returns to normal operating conditions.

130 In addition, the evolution of the perovskite structure when subjected to temperature cycles strongly
131 depends on the composition of the material. In the archetypical perovskite, MAPbI_3 , for example, the
132 cubic phase evolves to the tetragonal phase at temperatures below 327 K, with a further transition to
133 the orthorhombic phase below 162 K⁶⁰. Meanwhile, when the temperature reaches over 350 K, the
134 thermally-induced release of organic cations (MA^+) and vaporisation of the amine (MA) leads to the
135 degradation of the perovskite crystal^{61,62}. In FAMACs-based perovskite (FA = formamidinium)^{63,64},
136 the transition from the original cubic phase to the tetragonal phase occurs at ~ 240 K, whereas the
137 transition from the tetragonal to the orthorhombic phase does not occur above 100 K. The different
138 phase transition temperatures between these two perovskite compositions suggest that perovskite
139 composition is pivotal in determining its phase transition dynamics. In theory, maintaining the corner-
140 sharing assembly of the perovskite octahedral units in the 3D structure is critical to preserving its
141 optoelectronic properties. This understanding helps deepen insights into the perovskite structure,
142 directly impacting the device's reliability.

143 [H3] Strain

144 Beyond phase transitions, continuous lattice distortions can occur throughout the entire temperature
145 cycling process, and the lattice strain plays a central role^{65,66}. In solar cells, especially tandem cells, the
146 mismatch between the coefficients of thermal expansion (CTEs) of the absorber(s) and the
147 functioning layers will accordingly lead to a considerable non-uniformity in the strain distribution,
148 especially at the interfaces, under temperature cycling. In some severe cases, fast periodical
149 temperature changes can accelerate fatigue or even device failure due to the mechanical delamination
150 of the stack(s). In addition, each layer can also show variations in strain distribution, especially as a
151 function of the film thickness. The impact from the strain also varies by direction; for example, strain
152 along the out-of-plane direction is stronger and more releasable than in the in-plane direction due to

153 the presence of adjacent layers along the in-plane direction. This additional strain is concentrated on
154 the defective areas of the interface, leading to delamination after temperature cycling³². Compared to
155 fixed temperatures, thermal cycling introduces repetitive mechanical stress and generates dynamic
156 strain due to the constant expansion and contraction of layers with mismatched CTEs. Therefore,
157 these mechanical and interfacial challenges need to be addressed to improve the durability and
158 reliability of devices under dynamic operating conditions. The introduction of a heterochiral interface
159 has been validated to improve adhesion and mitigate fatigue under repeated thermal cycling (-40 to
160 +85 °C for 200 cycles), to address mechanical failures induced by mismatches in the CTEs⁶⁷. Future
161 research can build on such approaches to further enhance the long-term stability of perovskite-based
162 devices.

163 [H2] Impact on charge transport layers

164 Charge transport materials' (CTMs) characteristics have a substantial influence on the stability of
165 PSCs during temperature cycling, which brings into question whether the thermal stability of the
166 devices is due to the inherent thermal stability of the CTMs themselves. Indeed, CTMs that possess
167 robust thermal properties are associated with limited interfacial defect generation and have a
168 consistent energy level alignment with the perovskite layer across applied temperature ranges.
169 Employing poly[bis(4-phenyl)(2,4,6-trimethylphenyl)amine] (PTAA) instead of spiro-OMeTAD as
170 the CTM, for example, leads to sustained operational efficiency even at elevated temperatures because
171 of its low glass transition temperature^{68,69,70}. Nevertheless, temperature cycles have additional
172 implications on the material and device evolution, which are not only related to their intrinsic thermal
173 stability⁷¹.

174 Temperature cycling, in addition to a fixed high temperature, expedites interlayer material diffusion
175 due to the dynamic character of the system under consecutive temperature fluctuations. In particular,
176 ion migration is responsible for device instability due to degradation processes caused by ion
177 rearrangement in the perovskite films and/or redox chemical reactions between migrated ions,
178 especially halides, and active species in the devices⁷²⁻⁷⁵. In addition, the migration of ions departing
179 from perovskite films, that is, precursor cations and anions, can accelerate the degradation of the
180 transporting materials. For example, iodide from the perovskite layer can diffuse across the interface
181 into the adjacent layers. Similarly, metals in the top electrode, such as Ag, Au or Cu, can also diffuse
182 across the buffer and transport layers into the perovskite films⁷⁶. As material diffusion is largely
183 accelerated during temperature cycles, materials with conductivity values that show low dependence
184 on temperature should be chosen to mitigate performance decay.

185 CTLs should also have CTEs that are aligned with those of the perovskite layer. Within PSCs, the
186 attributes of individual materials in the different layers undergo dynamic fluctuations in response to
187 temperature cycles (**Fig. 2c**). Disparate CTEs between CTMs and perovskite lead to periodic

188 contractions and expansions at varying rates. When the CTL has a lower CTE than the perovskite
189 ($\sim 3.3 \times 10^{-5}$ to $8.4 \times 10^{-5} \text{ K}^{-1}$), the CTL constrains the perovskite along the in-plane directions during
190 cooling, resulting in in-plane tensile strain, especially a few nanometre deep in the perovskite layer.
191 Meanwhile, if the CTL has a higher CTE than the perovskite, the opposite may occur. Such interlayer
192 stress could potentially lead to the deformation of chemical bonds and to defect formation at the
193 interfaces, increasing the accumulation and recombination of charge carriers at defect sites and
194 subsequently decreasing the cell performance. In more severe instances, this mismatch may cause
195 delamination and/or fissure propagation, thereby substantially compromising both the efficiency and
196 durability of the devices^{77,78}. If the CTL is thin enough, the strain within the perovskite layer might be
197 negligible compared to the strain exerted by the thicker and stiffer substrate. In this case, the substrate
198 is dominant in controlling the strain in the perovskite. The stress caused by the mismatch in CTE may
199 be balanced by reducing or counteracting the forces between the compressive and tensile layers⁷⁹.
200 Using polymer substrates with CTEs closer to that of perovskite layers has been confirmed to well
201 mitigate stress caused by CTE mismatch⁷⁹.

202 [H2] Device performance following temperature cycling

203 Temperature cycles ultimately lead to changes in the PV performance of devices, which can be
204 reflected in the variations of the different device parameters: PCE, short-circuit current density (J_{SC}),
205 open-circuit voltage (V_{OC}), fill factor (FF), and hysteresis index (HI). The PCE values typically show
206 small variations under temperatures ranging from room temperature to +150 °C (**Fig. 3a**). As the
207 temperature decreases (from room temperature to -160 °C), however, the PCE begins to decrease,
208 showing an evolution pattern close to that of FF values, whereas the V_{OC} slightly increases. This
209 similarity suggests a tight relationship between the PCE and FF upon the decrease of the temperature,
210 which is likely associated with temperature-related charge extraction events. Unlike conventional
211 solar cells, the increased V_{OC} is not solely attributable to an enlarged bandgap (E_{g}) at low
212 temperatures, as the E_{g} of the perovskite decreases slightly with temperature cooling down⁶⁴. It is
213 rather linked to the suppression of trap-assisted non-radiative recombination in both the surface and
214 bulk of the perovskite layer. Meanwhile, the HI considerably increases as the temperature decreases,
215 which is evidenced by comparing the reverse and forward scans of J - V curves (**Fig. 3a**).

216 From the viewpoint of thermodynamic, the phase transition from the cubic to the tetragonal phase
217 with lowered temperature enables the effective elimination of intrinsic point defects in perovskite
218 films, extending the carrier lifetime and enhancing the V_{OC} in devices (**Fig. 3b-c**)⁶⁴. Intriguingly,
219 device performance is recoverable after a limited amount of temperature cycles, and the PCE can even
220 improve after one low-temperature cycle⁶⁴. J_{SC} , V_{OC} , and FF remain stable when returned to room
221 temperature after undergoing thermal cycles (**Fig. 3d**)³². This resilience may be linked to the

222 restoration of the perovskite structure following temperature fluctuations, which suggests that PSCs
223 have great potential in variable temperature environments, especially those that fluctuate around room
224 temperature. However, as the number of temperature cycles increases, the PCE starts to decline owing
225 to irreversible alterations in the device structure. These alterations include the accumulation of PbI_2 ,
226 the formation of the hexagonal phase in the perovskite layer, unreleased lattice strain, and decreased
227 transport capability and conductivity in CTLs.

228 Additionally, the evolution of the PV performance with temperature typically remains unaffected by
229 the intensity of the incident light, as suggested through a comparison of irradiation under AM1.5G
230 (standard solar spectrum on Earth's surface, approximately 1000 W/m^2) and AM0 (solar radiation in
231 outer space, approximately 1360 W/m^2) conditions³², or by the voltage. These results suggest that,
232 although additional stress factors like light and voltage influence the stability of PSCs, operational
233 stability under thermal cycling are mainly determined by the accumulation of irreversible changes in
234 the materials and devices due to temperature fluctuations. However, testing the cells under a
235 comprehensive combination of all the possible factors should be done to obtain global insights.

236 Because perovskite materials with different bandgaps exhibit varying properties, such as thermal
237 stability, ion migration behaviour, and mechanical stress tolerance, different responses under
238 temperature cycling are seen. Narrow-bandgap perovskites ($<1.5 \text{ eV}$), such as Sn-based or mixed Sn-
239 Pb perovskites, are considered ideal candidates for the bottom cell in tandem solar cells. However,
240 these Sn-containing perovskites are primarily sensitive to oxidation, either from oxygen invasion,
241 acidic poly(3,4-ethylenedioxythiophene)-poly(styrenesulfonate) (PEDOT:PSS)-induced I_2 generation,
242 or residual DMSO sourced from the solution processing of the films. Moreover, these processes can
243 be accelerated under thermal conditions, leading to device failure. Medium-bandgap perovskite
244 materials ($1.5\text{--}1.7 \text{ eV}$), which are primarily iodide-based (such as FAPbI_3) or low-bromide iodide
245 perovskites (when $\text{Br} < 20\%$), demonstrate relatively good thermal stability and are promising
246 candidates for use in extreme environments with large temperature fluctuations. Although phase
247 transitions and phase separation can still occur during temperature cycling, additive engineering or
248 interfacial modifications can considerably improve their thermal tolerance. For instance, perovskite
249 cells modified with β -poly(1,1-difluoroethylene) exhibited no signs of fatigue after 1000 hours of
250 maximum power point (MPP) tracking at $75 \text{ }^\circ\text{C}$ and thermal cycling between -60 and $+80 \text{ }^\circ\text{C}$ ⁵⁷.
251 Wide-bandgap perovskite materials ($>1.7 \text{ eV}$), such as FAPbBr_3 , exhibit a high population of defect
252 states and numerous ion migration events. However, the accumulation of ions in wide-bandgap
253 perovskite materials can result in phase separation, bandgap shifts and localized electric field failure
254 under temperature cycling, particularly at elevated temperatures⁸⁷. Enhancing thermal expansion
255 compatibility and developing self-healing perovskite materials offer promising approaches to mitigate
256 the degradation of wide-bandgap perovskites under cyclic temperature changes⁸⁸.

257 **[H1] Strategies to enhance the resilience of perovskite photovoltaics to temperature**
258 **cycling**

259 There are several strategies to enhance the stability of PSCs under temperature cycling. These
260 strategies encompass stabilizing the phase structure of the perovskites, either by improving the
261 crystallinity of the material or by reducing the lattice strain through the incorporation of buffer
262 materials at grain boundaries, mitigating defects using different modifications approaches, and
263 preventing delamination occurring within the perovskite layer itself and at its interfaces with the
264 CTLs by adopting thermally stable and highly conductive CTLs^{55,57,89-100}.

265 **[H2] Stabilizing the perovskite structure**

266 To ensure the stability of PSCs under temperature cycling, the crystalline stability of the perovskite
267 material must be maintained across the specified temperature range, thereby minimizing potential
268 irreversible effects of phase transitions during temperature fluctuations. As a strategy, molecules such
269 as β -poly(1,1-difluoroethylene) with an ordered dipole structure can regulate the crystallization and
270 energy level alignment of the perovskite film. By acting as molecular springs that dynamically
271 respond to stress within the perovskite lattice, these ordered molecules accommodate lattice strain
272 caused by thermal expansion or contraction, effectively stabilizing the crystal structure and mitigating
273 phase transitions. The device showed no signs of fatigue during rapid thermal cycling between -60
274 and $+80$ °C, highlighting the considerable impact of the ordered dipole structure on the operational
275 stability of perovskite solar cells⁵⁷. This is largely linked to the intrinsic stability of the perovskite
276 materials. For example, in the cases of FAPbI₃ and CsPbI₃, both the large FA⁺ ions and the small Cs⁺
277 ions induce distortions in the [PbX₆]⁴⁻ octahedra, resulting in deviations from the symmetric α -phase
278 (**Fig. 4a**). This structural distortion is a critical factor underpinning their phase instability¹⁰¹⁻¹⁰⁴. By
279 adjusting defect formation energy, lattice strain in perovskites can be controlled (**Fig. 4b**). Typically,
280 increasing compression stabilizes defects, while increasing tension destabilizes them. Consequently,
281 the inactive δ -phases possess the lowest free energy of formation at room temperature, rendering it
282 challenging to achieve stability under constant ambient conditions^{105,106}. The ionic structure of the
283 perovskite film is also critical in influencing device thermal stability, which is observed through phase
284 transitions in four standard perovskite materials in devices under thermal cycling between -30 and 85
285 °C¹⁰¹. Therefore, for materials like MAPbI₃ and mixed-cation perovskites, characterized by a certain
286 degree of stability at ambient conditions, meticulous attention must be paid to the dependency of
287 potential phase transitions to compositional variations. Notably, it was shown that adjustments in the
288 composition can lower the temperature required for phase transition between the cubic phase to
289 inactive phases at low temperatures, extending their applicability in cold environments^{63,64}.

290 [H2] Reducing lattice strain

291 The periphery of the substrate is subject to shear stress, a mechanical effect that is exacerbated by
292 variations in temperature. This phenomenon induces potentially greater displacements within the
293 perovskite lattice, consequently giving rise to lattice distortion or the formation of defects, thereby
294 impacting crucial material properties such as light absorption, charge transport, and carrier lifetime
295 (**Fig. 4c**). Moreover, it can promote alterations in the interface structure between the perovskite and
296 the substrate, thereby influencing interface charge transport dynamics and the sustained efficiency of
297 devices, particularly as they scale up in size¹⁰⁷. The challenge in addressing this issue predominantly
298 revolves around effectively mitigating and dispersing substrate-induced stress while concurrently
299 preserving the uniformity and structural integrity of the perovskite films (**Fig. 4d**). There is evidence
300 to suggest that rationally applied pressure can instigate phase transitions. Specifically, MAPbI₃ can
301 undergo phase transformation at pressures ranging from 0.3 to 0.4 GPa. The residual stress generated
302 during device fabrication can attain 77.7±5.4 MPa under constant room temperature conditions¹⁰⁰. It
303 was shown that an increase in environmental temperature from -40 to 85 °C led to a discernible
304 reduction in residual strain on the surface of the perovskite¹⁰⁰. Although this strain may not attain the
305 pressure threshold for phase transition, its evolution during thermal cycling can potentially impact
306 phase transition dynamics. This observation further explains why identical perovskite types exhibit
307 varying phase transition temperatures. Incorporating additives into either the perovskite precursor
308 solution or the antisolvent, which is used as quenching agent during wet device fabrication, facilitates
309 the formation of a dense film typified by larger grains owing to the resulting strain in the modified
310 structure. Such dense perovskite films have improved thermal cycle stability. Phase transition is also
311 related to the compactness of the perovskite; in general, the more compact the film is, the more stable
312 it is^{57,108-110}. Using a polymer as a buffer against thermomechanical stress at the crystal interfaces (**Fig.**
313 **4e**) improves the perovskite phase stability, suppresses ion diffusion, and produces minimal and
314 recoverable tension changes. Using this strategy, fabricated devices could maintain stable PV
315 performance during sustained thermal cycling between -60 and +80 °C for 120 cycles⁵⁷.

316 [H2] Improving the adhesion at the interfaces

317 Beyond improving the bulk properties of the perovskite material, it is imperative to regulate
318 detrimental strain and improve the adhesion at the interface between the CTL and the perovskite
319 material to enhance overall device performance. In this sense, an optimal alignment between the
320 CTEs of the perovskite layer and the adjacent layers can prevent fracture and premature delamination.
321 However, maintaining such alignment is challenging, especially considering the simultaneous CTL
322 selection requirements for efficiency optimization. Incorporating molecular interlayers to the stack of
323 the solar cell devices, based on flexible interconnecting molecules to bridge the perovskite and the
324 substrate, could alleviate delamination, thereby contributing to stabilise interfaces and suppress

325 mechanical failure^{49,83-86} (**Fig. 4f**). For instance, introducing a more pliable interlayer beneath the
326 perovskite layer, such as poly(methyl methacrylate) (PMMA), dimethylphenethylsulfonium iodide
327 (DMPEI), or ferrocenyl-bis-thiophene-2-carboxylate (FcTc2), between the perovskite and the CTL,
328 augment stability under thermal cycling conditions (**Fig. 4g**)^{21,55,111}. Specifically, PMMA as an
329 interfacial modification layer preserves the crystallinity of the device, which shows almost no
330 efficiency loss after 26 thermal cycles between 290 and 90 K⁹³. These interlayers, interfacing with
331 both the perovskite and CTLs, can modulate phase transition points by passivating defects and
332 alleviating interfacial stress. They can also increase adhesion^{84,112}, consequently increasing the
333 activation energy of ion migration. Additionally, the fracture energy can serve as a key figure of merit
334 for assessing the interfacial mechanical strength of perovskite devices⁸⁰⁻⁸². We believe fracture energy
335 could also be increased through mechanical reinforcement techniques or by integrating materials with
336 higher fracture toughness at the interfaces.

337 Enhancing the elasticity and mechanical stability of perovskites is another requirement for achieving
338 PSCs that are stable during thermal cycling. The introduction of interface buffer layers could stabilise
339 crystal-to-crystal and layer-to-layer contacts, leading to improved mechanical stability. A mechanistic
340 analysis of how the buffer layer alleviates interfacial stress in the perovskite and enhances the
341 device's thermal stability could offer valuable insights for developing new buffer layers. As an
342 example, a protonated aminosilane coupling agent, (OC₂H₅)₃-Si-(CH₂)₃-NH₃Br (PASCA-Br), was
343 used as a buffer layer between TiO₂ and a perovskite layer. The Si end anchors to the TiO₂ layer,
344 improving adhesion, whereas the R-NH₃Br end serves as a structural component to compensate for
345 defects in the perovskite's octahedral units, reducing lattice distortion. The R-NH₃Br extends the
346 growth sites, helping to release lattice stress, reducing in-plane strain from 1.55 to 0.67% and out-of-
347 plane stress from 1.47 to 0.73%. This strategy effectively mitigates interfacial strain, leading to
348 devices exhibiting higher carrier mobility in a broad temperature range from 223 to 263 K¹¹³. In
349 addition, incorporating dense, less penetrable buffer layers and/or less reactive electrodes, such as
350 carbon, or electrodes composed of material(s) capable of forming a diffusion barrier, such as
351 chromium,^{114,115} would be beneficial to mitigate material interdiffusion.

352 **[H1] Photovoltaic performance under real-world diurnal cycles**

353 Evaluating operational stability under field conditions is crucial before projecting perovskite PVs to
354 market, as⁵³ real-world results may differ from laboratory tests^{116,117}. This discrepancy was shown, for
355 example, after a one-year outdoor test in Berlin, where the outdoor operational stability of the device
356 was longer than when measured in conventional laboratory settings¹¹⁸. This result may be attributed to
357 the fact that switching between day and night enables devices to sufficiently recover during the night
358 via strain relaxation. The change of seasons also has a strong impact on the stability of PSCs; the PCE

359 drops from July to October and November to February, when the weather shows greater temperature
360 changes. PV performance is affected by the exposure to specific absolute temperature values (**Fig. 3**),
361 but prolonged times and consecutive cycles at high temperatures are much more detrimental for long-
362 term device stability (**Fig. 5a**). Meanwhile, other real-world stresses impact device stability⁵³.
363 Through a combination of computational simulations and data obtained from outdoor stability tests, it
364 was shown that high temperatures and light strongly determine the stability of PSCs under outdoor
365 conditions (**Fig. 5b-c**). This dependency can be caused by the photon-catalysed degradation of the
366 perovskite materials and the specific combination and compatibility of the layered materials involved
367 in the devices. In this case, the behaviour observed in lab tests correlated with field conditions,
368 enabling the use of indoor accelerated stability tests to predict device performance under outdoor
369 ageing. For the particular case of p-i-n (inverted) PSCs, to improve their stability under temperature
370 cycles and outdoor conditions, a mixture of self-assembled monolayers can be used to improve the
371 interface. Considering the influence of other environmental factors (such as humidity or even
372 rainwater), advancing encapsulation is critical¹¹⁷. The PCE of perovskite/silicon tandem solar cells is
373 also strongly dependent to the cyclic nature of operational conditions¹¹⁹⁻¹²¹.

374 In particular, we would like to highlight the dependency of the bandgap of the absorber layers to
375 temperature, which leads to variability in the optimal values needed for current matching¹¹⁹. Firstly, in
376 perovskite-silicon tandem cells, the optimal bandgap for current matching is about 1.73 eV. However,
377 the c-Si bandgap undergoes a redshift as the temperature increases, whereas the perovskite bandgap
378 undergoes a blueshift, thereby leading to energy level misalignment in the device and impacting its
379 efficiency¹¹⁹. Secondly, when tandem cells are deployed in real-world environments, temperature
380 fluctuations or external forces may induce stress within the thin films. Experimental results have
381 shown that when the temperature drops from 80 to 30 °C, the tensile stress in the perovskite film can
382 reach as high as 87.66 MPa¹²². If the compressive stress exceeds the critical stress, it can lead to layer
383 failure or delamination¹²³. Moreover, bottom texturization, such as the use of random pyramid
384 textures, substantially improves light coupling efficiency¹²⁴. The top and bottom cells can be
385 interconnected via a nanocrystalline silicon composite junction, combining low tunnel resistance and
386 high shunt elasticity to fully couple near-infrared light into the c-Si bottom cell¹²⁵, thereby addressing
387 the effect of temperature-induced bandgap changes in perovskite and c-Si on tandem cell
388 performance. Using a textured silicon surface structure with no sharp angles can additionally alleviate
389 stress concentration issues during thermal cycling¹²⁶. Furthermore, adjusting the size of A-site ions in
390 the perovskite, such as modifying the content of MA⁺, Rb⁺, or Cs⁺ at the A-site, can help relieve the
391 stress between the perovskite and silicon layers^{127,128}.

392 [H1] Stability assessment protocols

393 To better quantify the temperature sensitivity of the performance of PV devices and compare PV
394 parameters variation in different works, the temperature coefficient $\beta_G(T)$ has been introduced^{129,130},
395 which characterises the variation of a parameter G (V_{OC} , J_{SC} , FF or PCE) as a function of temperature
396 T :

$$397 \quad \beta_G(T) = \frac{10^6}{G(T_0)} \frac{G(T) - G(T_0)}{T - T_0} \quad (1)$$

398 where T_0 is room temperature (298.15 K) and the temperature coefficients are expressed in ppm K⁻¹.

399 As reported, in PSCs, the decline of V_{OC} with increasing temperature is lower than that for silicon
400 solar cells⁶⁴. This result, in theory, suggests that PSCs could present higher operational thermal
401 stability, particularly under temperature cycling conditions.

402 For the long-term stability test of devices, the perovskite PV research community has constructed test
403 standards based on the International Summit on Organic PV Stability (ISOS)^{19,56,131}. As the study of
404 stability under temperature cycling is still in its early stage, applying unified test evaluation
405 procedures is particularly important. There are already some protocols related to measuring devices
406 under temperature cycles, such as ISOI-T-1, ISOI-T-2, and ISOI-T-3¹⁹ (**Table 1**). However, these
407 protocols consider too narrow temperature ranges for certain applications and have limited guidelines
408 on other parameters such as the heating and cooling rates. The temperature range suggested by the
409 ISOI-T-3 protocol goes from -45 to +85 °C, which is enough to simulate most terrestrial applications.
410 Meanwhile, for applications in extreme-temperature earth regions and space environments, a broader
411 cycling temperature range is required^{36,132}. In space, the absence of atmosphere and resulting lack of
412 heat transfer can cause the surface temperature of aircraft to fluctuate rapidly and considerably
413 between darkness and sunlight. We suggest adopting a wide temperature test range of -160 to 150
414 °C^{32,133}. In addition to specifying the temperature range for the thermal cycle, it is also important to
415 establish guidelines for the temperature ramp rate, cooling rate, and dwell time at specific
416 temperatures. Rapid heating and cooling rates can generate substantial thermal stress within the cell
417 materials. When temperature changes occur too rapidly, the materials may not expand or contract at
418 the comparable rate, leading to increased mechanical stress that can cause microcracks, interfacial
419 failure, or delamination between layers. Therefore, in addition to defining the temperature range for
420 thermal cycling, it is crucial to incorporate heating and cooling rates, as well as specific
421 environmental temperature cycles, into the thermal cycling test protocols. Under light irradiation and
422 at night or when shaded, the simulated accelerated heating or cooling rate could be set more broad to

423 provide a better approximation of rapid day-night temperature fluctuations, for instance an accelerated
424 thermal cycling protocol with a 20 °C/min ramp rate and a 2-minute thermal equilibrium hold
425 between -60 and +80 °C. This protocol, in addition to established standards (such as ISOS), should
426 expedite the detection of potential failure modes under fluctuating temperatures, providing faster
427 stability insights and identifying weaknesses within devices and encapsulation materials. Notably, this
428 protocol has demonstrated effectiveness in correlating accelerated perovskite degradation with device
429 thermal cycling stability⁵⁷. Additionally, humidity variations can accelerate material degradation,
430 making it essential to include humidity changes in thermal cycling tests. For instance, in inland basin
431 regions, intense solar radiation during the day leads to rapid temperature increases and a drop in
432 humidity, while at night, radiative cooling causes substantial temperature drops and an increase in
433 humidity. This effect is even more pronounced in extremely dry regions, such as deserts, where
434 fluctuations in temperature and humidity are more extreme. Therefore, we recommend incorporating
435 humidity variation as a key parameter in thermal cycling protocols to more accurately simulate real-
436 world conditions and properly evaluate the impact of temperature and humidity on device
437 performance, ensuring comprehensive test results.

438 As a reference, **Fig. 6** presents a recommended temperature cycle profile ranging from -40 to +85 °C,
439 as outlined in the IEC 61215 standard^{134,135}. It suggests a cooling and heating rate during the cycles
440 ranging between 45 and 100 °C h⁻¹ (0.75 and 1.67 °C min⁻¹), with a >10 min dwell time, and a
441 duration for one cycle ideally shorter than 6 h. Also, the applied current during the thermal process
442 can cause local heating in solar cells, potentially inducing high series resistance exceeding the
443 maximum set temperature. The current magnitude depends on the kinds of absorber materials. When
444 characterizing different properties under temperature cycles, it is advisable to indicate the specific
445 temperature and the number of temperature cycles applied. Additionally, the long-term stability may
446 exhibit varying rates when devices are subjected to different temperature intervals⁵⁷.

447 **[H1] Outlook**

448 The research on accelerated ageing of PSCs through thermal cycling tests has been relatively limited
449 in comparison to constant temperature measurements. Nevertheless, the more and more evident
450 commercialization potential of perovskite PV is gradually encouraging more studies in this direction.
451 Compared to fixed temperatures, temperature cycles have very different impacts on the evolution of
452 the perovskite materials and PV devices. Hence, efforts to unravel the underlying mechanisms of
453 temperature cycling in PSCs and to develop stable and high-efficient perovskite devices under
454 temperature cycles are still needed. Here, we point out four avenues for improving perovskite stability
455 under temperature cycling and provide suggestions for more realistic temperature cycle stability
456 testing in the future.

457 The first strategy to improve stability would be to explore more effective and robust ligands with
458 multiple anchoring groups, such as polymers, to serve as strain buffers for adjacent layers with
459 different CTEs and inhibit ion migration between the stack layers. While this approach has been
460 investigated in some studies, its impact under temperature cycling conditions has not been extensively
461 explored, leaving room for further validation in practical scenarios. As a valid strategy to increase the
462 thermal stability of PSCs, achieving robust energy level alignment under temperature cycling is also
463 important to maintain photoconversion efficiency, complementing the function of strain-buffering
464 ligands.

465 Secondly, selecting an appropriate CTL is crucial to achieving device stability during temperature
466 cycling. Higher temperatures in the cycling process can have a greater impact on certain organic
467 transport layers, such as Spiro-OMeTAD, which may degrade up to +70 °C¹³⁶. Besides considering
468 the thermal stability of the CTL itself, its CTE should also be considered. It is recommended to
469 choose one that closely matches that of the perovskite layer to prevent delamination between the two
470 layers during temperature cycles. Alternatives such as PTAA offer better thermal stability and closer
471 CTE matching with perovskites, while inorganic options like NiO_x provide exceptional thermal
472 stability and interface robustness. Additionally, self-assembled monolayers (SAMs), as one of the
473 leading HTL candidates, present challenges under elevated temperatures where bond breakage may
474 occur. Enhancing their binding properties under thermal stress will be a significant milestone in
475 promoting stable perovskite photovoltaics. Evaluating CTLs based on their thermal behaviour, CTE
476 compatibility, and durability under cycling conditions is essential for improving the performance and
477 longevity of perovskite solar cells.

478 Thirdly, encapsulation greatly affects the lifetime of devices as it suppresses the internal degradation
479 of volatile species and the external ingress of moisture and reactive species. Significant progress
480 has been made in this area, with materials such as ethylene vinyl acetate (EVA), polyvinyl butyral
481 (PVB) and polyisobutylene (PIB) demonstrating the ability to create effective moisture barriers.
482 These materials are selected based on characteristics, such as their elastic modulus, morphology, and
483 CTE mismatches with the perovskite^{49,137,138}. However, challenges remain in achieving encapsulation
484 materials that combine long-term stability with resistance to dynamic thermal cycling. For instance, a
485 rigid encapsulation material possibly departs the perovskite solar cells during thermal cycling, leading
486 to mechanical failure. Future research should focus on developing encapsulation systems with
487 enhanced barrier properties, self-healing mechanisms, and better compatibility with perovskite layers
488 to address delamination and moisture ingress over time. Therefore, suitable encapsulant materials and
489 techniques are highly needed to enhance thermal cycling stability and improve the commercial
490 viability of the device by reducing the impact of temperature cycling on the entire device. It is also
491 important to conduct thermal cycling tests on fully encapsulated devices to evaluate and study the
492 mechanisms involved during temperature cycling.

493 Finally, the decomposition mechanism of PSCs under temperature cycles remains underexplored. To
494 gain a better understanding of its behaviour, it is crucial to employ consistent and uniform testing
495 methods. Given that high temperatures typically coincide with sunlight exposure, and low
496 temperatures normally occur at nighttime, it would be more meaningful to study the working
497 performance of PSCs at high temperatures and their storage and/or self-healing performance at low or
498 room temperatures within thermal cycling. This approach would provide valuable insights into the
499 behaviour and stability of PSCs under realistic operating conditions. By examining the performance
500 of solar devices during both high-temperature operation and low-temperature storage and/or recovery,
501 researchers can gather comprehensive knowledge relevant to practical applications and address the
502 challenges associated with temperature cycling more effectively. Additionally, to better study the
503 working mechanism of PSCs in real life, other stress combination, such as temperature with humidity,
504 bias or atmosphere should be considered in future research.

505

506 **Acknowledgements**

507 This review is supported by the European Research Council (ERC) under the European Union's
508 Horizon 2020 research and innovation programme (grant agreement No. 804519), the European
509 Union's Horizon Europe research and innovation programme under grant agreement No. 101075330
510 of the NEXUS project, the Marie Skłodowska Curie Actions Postdoc Fellow (UKRI Guarantee, grant
511 number EP/Y029216/1). S.H.T.C. would like to thank the funding support of the Ministry of Science
512 and Innovation of Spain under Ayudas Ramón y Cajal (RYC2022-035578-I). J. P. acknowledges
513 support from Energy for future – E4F Postdoctoral fellowship program H2020-MSCA-COFUND-
514 2020 (101034297). M.S. thanks the German Research Foundation (DFG) for funding (SPP2196,
515 431314977/GRK 2642). GRK: “funded by the Deutsche Forschungsgemeinschaft (DFG, German
516 Research Foundation) - 431314977/GRK2642”. M.S. acknowledges funding from the European
517 Union under the Horizon Europe programme (ERC, LOCAL-HEAT, grant agreement No.
518 101041809). M.S. acknowledges funding from the German Bundesministerium für Bildung and
519 Forschung (BMBF), project “NETPEC” (01LS2103E). Views and opinions expressed are, however,
520 those of the author(s) only and do not necessarily reflect those of the European Union or the European
521 Research Council. Neither the European Union nor the granting authority can be held responsible for
522 them.

523 **Author contributions**

524 L.W., S.H., F.Y. and G.L. contributed to the writing and editing of this manuscript. L.W. and G.L.
525 prepared the first draft. G.L. and M.L. contributed to the discussion of content and writing. A.A.
526 contributed to the discussion and review of the manuscript. G.L., J.P., M.L. and A.A. supervised the

527 project. S.H., F.Y., J.W., W.Z., J.J.J.R., J.P. and S.H.T.C. contributed to suggestions and revised the
528 manuscript. M.S., M.S. and M.K.N. reviewed and edited the manuscript. All authors contributed their
529 expertise and participated in revision rounds of the manuscript.

530 **Competing interests**

531 The authors declare no competing interests.

532 **Peer review information**

533 *Nature Reviews XXX* thanks [Referee#1 name], [Referee#2 name] and the other, anonymous,
534 reviewer(s) for their contribution to the peer review of this work.

535

536 **References**

- 537 1 Green, M. A., Ho-Baillie, A. & Snaith, H. J. The emergence of perovskite solar cells. *Nature*
538 *Photonics* **8**, 506-514,(2014).
- 539 2 Saliba, M. *et al.* Incorporation of rubidium cations into perovskite solar cells improves
540 photovoltaic performance. *Science* **354**, 206-209,(2016).
- 541 3 De Wolf, S. *et al.* Organometallic Halide Perovskites: Sharp Optical Absorption Edge and Its
542 Relation to Photovoltaic Performance. *The Journal of Physical Chemistry Letters* **5**, 1035-
543 1039,(2014).
- 544 4 Wu, L. *et al.* Stabilization of Inorganic Perovskite Solar Cells with a 2D Dion–Jacobson
545 Passivating Layer. *Advanced Materials* **35**, 2304150-2304150,(2023).
- 546 5 Huang, W., Bu, T., Huang, F. & Cheng, Y. B. Stabilizing High Efficiency Perovskite Solar
547 Cells with 3D-2D Heterostructures. *Joule* **4**, 975-979,(2020).
- 548 6 Saliba, M., Correa-Baena, J.-P., Grätzel, M., Hagfeldt, A. & Abate, A. Perovskite Solar Cells:
549 From the Atomic Level to Film Quality and Device Performance. *Angewandte Chemie*
550 *International Edition* **57**, 2554-2569,(2018).
- 551 7 Liu, D. & Kelly, T. L. Perovskite solar cells with a planar heterojunction structure prepared
552 using room-temperature solution processing techniques. *Nature Photonics* **8**, 133-138,(2014).
- 553 8 Stranks, S. D. & Snaith, H. J. Metal-halide perovskites for photovoltaic and light-emitting
554 devices. *Nature Nanotechnology* **10**, 391-402,(2015).
- 555 9 Liu, M., Johnston, M. B. & Snaith, H. J. Efficient planar heterojunction perovskite solar cells
556 by vapour deposition. *Nature* **501**, 395-398,(2013).
- 557 10 Nandi, P. *et al.* CH₃NH₃PbI₃, A Potential Solar Cell Candidate: Structural and Spectroscopic
558 Investigations. *The Journal of Physical Chemistry A* **120**, 9732-9739,(2016).
- 559 11 NREL Transforming ENERGY, <https://www.nrel.gov/pv/cell-efficiency.html>
- 560 12 Liu, S. *et al.* Buried interface molecular hybrid for inverted perovskite solar cells. *Nature* **632**,
561 536-542,(2024).
- 562 13 Peters, I. M., Rodríguez Gallegos, C. D., Lüer, L., Hauch, J. A. & Brabec, C. J. Practical
563 limits of multijunction solar cells. *Prog. Photovoltaics* **31**, 1006-1015,(2023).

564 14 McMeekin, D. P. *et al.* A mixed-cation lead mixed-halide perovskite absorber for tandem
565 solar cells. *Science* **351**, 151-155,(2016).

566 15 Stranks, S. D. *et al.* Electron-hole diffusion lengths exceeding 1 micrometer in an
567 organometal trihalide perovskite absorber. *Science* **342**, 341-344,(2013).

568 16 Green, M. A. *et al.* Solar cell efficiency tables (Version 64). *Prog. Photovoltaics* **32**, 425-441,
569 (2024).

570 17 Luo, L. *et al.* Stabilization of 3D/2D perovskite heterostructures via inhibition of ion diffusion
571 by cross-linked polymers for solar cells with improved performance. *Nature Energy* **8**, 294-
572 303,(2023).

573 18 Turren-Cruz, S.-H., Hagfeldt, A. & Saliba, M. Methylammonium-free, high-performance, and
574 stable perovskite solar cells on a planar architecture. *Science* **362**, 449-453,(2018).

575 19 Khenkin, M. V. *et al.* Consensus statement for stability assessment and reporting for
576 perovskite photovoltaics based on ISOS procedures. *Nature Energy* **5**, 35-49,(2020).

577 20 Jeronimo-Rendon, J. J. *et al.* Robust Multi-Halide Methylammonium-Free Perovskite Solar
578 Cells on an Inverted Architecture. *Advanced Functional Materials* **n/a**, 2313928-2313928,
579 (2024).

580 21 Li, Z. *et al.* Organometallic-functionalized interfaces for highly efficient inverted perovskite
581 solar cells. *Science* **376**, 416-420,(2022).

582 22 Chen, R. *et al.* Reduction of bulk and surface defects in inverted methylammonium- and
583 bromide-free formamidinium perovskite solar cells. *Nature Energy* **8**, 839-849,(2023).

584 23 Yang, Y. *et al.* Inverted perovskite solar cells with over 2,000 h operational stability at 85 °C
585 using fixed charge passivation. *Nat. Energy* **9**, 37-46Nature Reviews Materials,(2023).

586 24 Li, G. *et al.* Managing Excess Lead Iodide with Functionalized Oxo-Graphene Nanosheets for
587 Stable Perovskite Solar Cells. *Angewandte Chemie International Edition* **135**, e202307395-
588 e202307395,(2023).

589 25 Wang, M. *et al.* Ammonium cations with high pKa in perovskite solar cells for improved
590 high-temperature photostability. *Nature Energy* **8**, 1229-1239,(2023).

591 26 Li, H. *et al.* 2D/3D heterojunction engineering at the buried interface towards high-
592 performance inverted methylammonium-free perovskite solar cells. *Nature Energy* **8**, 946-
593 955,(2023).

594 27 Jiang, Q. *et al.* Surface reaction for efficient and stable inverted perovskite solar cells. *Nature*
595 **611**, 278-283,(2022).

596 28 Zhu, K. & Stranks, S. D. Energy Spotlight. *ACS Energy Letters* **7**, 1862-1863,(2022).

597 29 Park, S. M. *et al.* Engineering ligand reactivity enables high-temperature operation of stable
598 perovskite solar cells. *Science* **381**, 209-215,(2023).

599 30 Li, C. *et al.* Rational design of Lewis base molecules for stable and efficient inverted
600 perovskite solar cells. *Science* **379**, 690-694,(2023).

601 31 Peng, W. *et al.* Reducing nonradiative recombination in perovskite solar cells with a porous
602 insulator contact. *Science* **379**, 683-690,(2023).

603 32 Li, G. *et al.* Structure and Performance Evolution of Perovskite Solar Cells under Extreme
604 Temperatures. *Advanced Energy Materials* **12**, 2202887-2202887,(2022).

605 33 Sharma, N. *et al.* Solar power forecasting beneath diverse weather conditions using GD and
606 LM-artificial neural networks. *Scientific Reports* **13**, 8517-8517,(2023).

607 34 Akbulatov, A. F. *et al.* Effect of Electron-Transport Material on Light-Induced Degradation
608 of Inverted Planar Junction Perovskite Solar Cells. *Advanced Energy Materials* **7**, 1700476-
609 1700476,(2017).

610 35 De Bastiani, M. *et al.* Toward Stable Monolithic Perovskite/Silicon Tandem Photovoltaics: A
611 Six-Month Outdoor Performance Study in a Hot and Humid Climate. *ACS Energy Letters* **6**,
612 2944-2951,(2021).

613 36 Tu, Y. *et al.* Perovskite Solar Cells for Space Applications: Progress and Challenges.
614 *Advanced Materials* **33**, 2006545-2006545,(2021).

615 37 Brown, C. R., Eperon, G. E., Whiteside, V. R. & Sellers, I. R. Potential of High-Stability
616 Perovskite Solar Cells for Low-Intensity–Low-Temperature (LILT) Outer Planetary Space
617 Missions. *ACS Applied Energy Materials* **2**, 814-821,(2019).

618 38 Park, S. M. *et al.* Low-loss contacts on textured substrates for inverted perovskite solar cells.
619 *Nature* **624**, 289-294,(2023).

620 39 Reb, L. K. *et al.* Perovskite and Organic Solar Cells on a Rocket Flight. *Joule* **4**, 1880-1892,
621 (2020).

622 40 Barbé, J. *et al.* In situ investigation of perovskite solar cells' efficiency and stability in a
623 mimic stratospheric environment for high-altitude pseudo-satellites. *Journal of Materials*
624 *Chemistry C* **8**, 1715-1721,(2020).

625 41 Romano, V., Agresti, A., Verduci, R. & D'Angelo, G. Advances in Perovskites for
626 Photovoltaic Applications in Space. *ACS Energy Letters* **7**, 2490-2514,(2022).

627 42 Yang, J., Bao, Q., Shen, L. & Ding, L. Potential applications for perovskite solar cells in
628 space. *Nano Energy* **76**, 105019-105019,(2020).

629 43 Ma, Q., Liao, S., Ma, Y., Chu, Y. & Wang, Y. An Ultra-Low-Temperature Elastomer with
630 Excellent Mechanical Performance and Solvent Resistance. *Advanced Materials* **33**, 2102096-
631 2102096,(2021).

632 44 Panteli, M. & Mancarella, P. Influence of extreme weather and climate change on the
633 resilience of power systems: Impacts and possible mitigation strategies. *Electric Power*
634 *Systems Research* **127**, 259-270,(2015).

635 45 Al-Shahri, O. A. *et al.* Solar photovoltaic energy optimization methods, challenges and issues:
636 A comprehensive review. *Journal of Cleaner Production* **284**, 125465-125465,(2021).

637 46 Gernaat, D. E. H. J. *et al.* Climate change impacts on renewable energy supply. *Nature*
638 *Climate Change* **11**, 119-125,(2021).

639 47 Tu, Y. *et al.* Mixed-cation perovskite solar cells in space. *Science China Physics, Mechanics*
640 *& Astronomy* **62**, 974221-974221,(2019).

641 48 Wang, X. *et al.* Elimination of charge accumulation by a self-assembled cocrystal interlayer
642 for efficient and stable perovskite solar cells. *Energ. Environ. Sci.* **17**, 569-579,(2024).

643 49 Checharoen, R. *et al.* Design and understanding of encapsulated perovskite solar cells to
644 withstand temperature cycling. *Energy & Environmental Science* **11**, 144-150,(2018).

645 50 Guo, R. *et al.* Degradation mechanisms of perovskite solar cells under vacuum and one
646 atmosphere of nitrogen. *Nature Energy* **6**, 977-986,(2021).

647 51 Domanski, K., Alharbi, E. A., Hagfeldt, A., Grätzel, M. & Tress, W. Systematic investigation
648 of the impact of operation conditions on the degradation behaviour of perovskite solar cells.
649 *Nature Energy* **3**, 61-67,(2018).

650 52 Zhou, Y., Herz, L. M., Jen, A. K. Y. & Saliba, M. Advances and challenges in understanding
651 the microscopic structure–property–performance relationship in perovskite solar cells. *Nature*
652 *Energy* **7**, 794-807,(2022).

653 53 Jiang, Q. *et al.* Towards linking lab and field lifetimes of perovskite solar cells. *Nature* **623**,
654 313–318,(2023).

655 54 Li, X. *et al.* Iodine-trapping strategy for light-heat stable inverted perovskite solar cells under
656 ISOS protocols. *Energy & Environmental Science* **16**, 6071-6077,(2023).

657 55 Suo, J. *et al.* Multifunctional sulfonium-based treatment for perovskite solar cells with less
658 than 1% efficiency loss over 4,500-h operational stability tests. *Nat. Energy* **9**, 172–183,
659 (2024).

660 56 Khenkin, M. *et al.* Light cycling as a key to understanding the outdoor behaviour of
661 perovskite solar cells. *Energy & Environmental Science*,(2024).

662 57 Li, G. *et al.* Highly efficient p-i-n perovskite solar cells that endure temperature variations.
663 *Science* **379**, 399-403,(2023).

664 58 Li, Z., Park, J. S. & Walsh, A. Evolutionary exploration of polytypism in lead halide
665 perovskites. *Chem Sci* **12**, 12165-12173,(2021).

666 59 Domanski, K. *et al.* Migration of cations induces reversible performance losses over day/night
667 cycling in perovskite solar cells. *Energy & Environmental Science* **10**, 604-613,(2017).

668 60 Hoang, M. T., Yang, Y., Tuten, B. & Wang, H. Are Metal Halide Perovskite Solar Cells
669 Ready for Space Applications? *J. Phys. Chem. Lett.* **13**, 2908-2920,(2022).

670 61 Juarez-Perez, E. J., Hawash, Z., Raga, S. R., Ono, L. K. & Qi, Y. Thermal degradation of
671 CH₃NH₃PbI₃ perovskite into NH₃ and CH₃I gases observed by coupled thermogravimetry–
672 mass spectrometry analysis. *Energy & Environmental Science* **9**, 3406-3410,(2016).

673 62 Ava, T. T., Al Mamun, A., Marsillac, S. & Namkoong, G. A Review: Thermal Stability of
674 Methylammonium Lead Halide Based Perovskite Solar Cells. *Applied SciencesProgress in*
675 *Photovoltaics: Research and Applications* **9** (2019).

676 63 Weber, O. J., Charles, B. & Weller, M. T. Phase behaviour and composition in the
677 formamidinium–methylammonium hybrid lead iodide perovskite solid solution. *Journal of*
678 *Materials Chemistry A* **4**, 15375-15382,(2016).

679 64 Chen, Y. *et al.* Self-Elimination of Intrinsic Defects Improves the Low-Temperature
680 Performance of Perovskite Photovoltaics. *Joule* **4**, 1961-1976,(2020).

681 65 Meng, W. *et al.* Revealing the strain-associated physical mechanisms impacting the
682 performance and stability of perovskite solar cells. *Joule* **6**, 458-475,(2022).

683 66 Wu, J. *et al.* Strain in perovskite solar cells: origins, impacts and regulation. *National Science*
684 *Review* **8**, nwab047-nwab047,(2021).

685 67 Duan, T. *et al.* Chiral-structured heterointerfaces enable durable perovskite solar cells. **384**,
686 878-884,(2024).

687 68 Malinauskas, T. *et al.* Enhancing Thermal Stability and Lifetime of Solid-State Dye-
688 Sensitized Solar Cells via Molecular Engineering of the Hole-Transporting Material Spiro-
689 OMeTAD. *ACS Applied Materials & Interfaces* **7**, 11107-11116,(2015).

690 69 Zhao, X., Kim, H.-S., Seo, J.-Y. & Park, N.-G. Effect of Selective Contacts on the Thermal
691 Stability of Perovskite Solar Cells. *ACS Applied Materials & Interfaces* **9**, 7148-7153,(2017).

692 70 Jena, A. K., Numata, Y., Ikegami, M. & Miyasaka, T. Role of spiro-OMeTAD in
693 performance deterioration of perovskite solar cells at high temperature and reuse of the
694 perovskite films to avoid Pb-waste. *J. Mater. Chem. A* **6**, 2219-2230,(2018).

695 71 Divitini, G. *et al.* In situ observation of heat-induced degradation of perovskite solar cells.
696 *Nature Energy* **1**, 15012-15012,(2016).

697 72 Snaith, H. J. *et al.* Anomalous Hysteresis in Perovskite Solar Cells. *J Phys Chem Lett* **5**, 1511-
698 1515,(2014).

699 73 Unger, E. L. *et al.* Hysteresis and transient behavior in current–voltage measurements of
700 hybrid-perovskite absorber solar cells. *Energ. Environ. Sci.* **7**, 3690-3698,(2014).

701 74 Tress, W. *et al.* Understanding the rate-dependent J–V hysteresis, slow time component, and
702 aging in CH₃NH₃PbI₃ perovskite solar cells: the role of a compensated electric field. *Energ.*
703 *Environ. Sci.* **8**, 995-1004,(2015).

704 75 Yang, T.-Y., Gregori, G., Pellet, N., Grätzel, M. & Maier, J. The Significance of Ion
705 Conduction in a Hybrid Organic–Inorganic Lead-Iodide-Based Perovskite Photosensitizer.
706 *Angewandte Chemie International Edition* **54**, 7905-7910,(2015).

707 76 Zhang, D., Li, D., Hu, Y., Mei, A. & Han, H. Degradation pathways in perovskite solar cells
708 and how to meet international standards. *Communications Materials* **3**, 58,(2022).

709 77 Ma, S. *et al.* Development of encapsulation strategies towards the commercialization of
710 perovskite solar cells. *Energ. Environ. Sci.* **15**, 13-55,(2022).

711 78 Dong, Q. *et al.* Interpenetrating interfaces for efficient perovskite solar cells with high
712 operational stability and mechanical robustness. *Nat. Commun.* **12**, 973,(2021).

713 79 McAndrews, G. R. *et al.* Why Perovskite Thermal Stress is Unaffected by Thin Contact
714 Layers. *Advanced Energy Materials* **14**, 2400764,(2024).

715 80 Hilt, F. *et al.* Rapid route to efficient, scalable, and robust perovskite photovoltaics in air.
716 *Energy & Environmental Science* **11**, 2102-2113,(2018).

717 81 Liu, D. *et al.* Strain analysis and engineering in halide perovskite photovoltaics. *Nature*
718 *Materials* **20**, 1337-1346,(2021).

719 82 Dai, Z. & Padture, N. P. Challenges and opportunities for the mechanical reliability of metal
720 halide perovskites and photovoltaics. *Nature Energy* **8**, 1319-1327,(2023).

721 83 Dai, Z. *et al.* Interfacial toughening with self-assembled monolayers enhances perovskite
722 solar cell reliability. *Science* **372**, 618-622,(2021).

723 84 Dai, Z. *et al.* Connecting Interfacial Mechanical Adhesion, Efficiency, and Operational
724 Stability in High Performance Inverted Perovskite Solar Cells. *ACS Energy Letters* **9**, 1880-
725 1887,(2024).

726 85 Watson, B. L., Rolston, N., Printz, A. D. & Dauskardt, R. H. Scaffold-reinforced perovskite
727 compound solar cells. *Energy & Environmental Science* **10**, 2500-2508,(2017).

728 86 Rolston, N. *et al.* Rapid Open-Air Fabrication of Perovskite Solar Modules. *Joule* **4**, 2675-
729 2692,(2020).

730 87 Chen, C. *et al.* Arylammonium-Assisted Reduction of the Open-Circuit Voltage Deficit in
731 Wide-Bandgap Perovskite Solar Cells: The Role of Suppressed Ion Migration. *ACS Energy*
732 *Letters* **5**, 2560-2568,(2020).

733 88 Liu, J. *et al.* Mitigating deep-level defects through a self-healing process for highly efficient
734 wide-bandgap inorganic CsPbI₃–xBr_x perovskite photovoltaics. *Journal of Materials*
735 *Chemistry A* **10**, 17237-17245,(2022).

736 89 Shi, P. *et al.* Oriented nucleation in formamidinium perovskite for photovoltaics. *Nature* **620**,
737 323-327,(2023).

738 90 Tan, Q. *et al.* Inverted perovskite solar cells using dimethylacridine-based dopants. *Nature*
739 **620**, 545-551,(2023).

740 91 Li, F. *et al.* Hydrogen-bond-bridged intermediate for perovskite solar cells with enhanced
741 efficiency and stability. *Nature Photonics* **17**, 478-484,(2023).

742 92 Jiang, Q. *et al.* Compositional texture engineering for highly stable wide-bandgap perovskite
743 solar cells. *Science* **378**, 1295-1300,(2022).

744 93 Qiu, W. *et al.* Low-Temperature robust MAPbI₃ perovskite solar cells with power conversion
745 efficiency exceeding 22.4%. *Chemical Engineering Journal* **468**, 143656-143656,(2023).

746 94 Wang, S. *et al.* In Situ Self-Elimination of Defects via Controlled Perovskite Crystallization
747 Dynamics for High-Performance Solar Cells. *Advanced Materials* **35**, 2305314-2305314,
748 (2023).

749 95 You, S. *et al.* Bifunctional hole-shuttle molecule for improved interfacial energy level
750 alignment and defect passivation in perovskite solar cells. *Nature Energy* **8**, 515-525,(2023).

751 96 Zhang, C. *et al.* Crystallization manipulation and holistic defect passivation toward stable and
752 efficient inverted perovskite solar cells. *Energy & Environmental Science* **16**, 3825-3836,
753 (2023).

754 97 Liu, C. *et al.* Bimolecularly passivated interface enables efficient and stable inverted
755 perovskite solar cells. *Science* **382**, 810-815,(2023).

756 98 Yu, S. *et al.* Homogenized NiOx nanoparticles for improved hole transport in inverted
757 perovskite solar cells. *Science* **382**, 1399-1404,(2023).

758 99 Wang, C. *et al.* Enhancing the Inherent Stability of Perovskite Solar Cells through
759 Chalcogenide-Halide Combinations. *Energ. Environ. Sci.* **17**, 1368-1386,(2024).

760 100 Wang, H. *et al.* Interfacial Residual Stress Relaxation in Perovskite Solar Cells with
761 Improved Stability. *Advanced Materials* **31**, 1904408-1904408,(2019).

762 101 He, J. *et al.* Influence of phase transition on stability of perovskite solar cells under thermal
763 cycling conditions. *Solar Energy* **188**, 312-317,(2019).

764 102 Yang, B. *et al.* Strain effects on halide perovskite solar cells. *Chem Soc Rev* **51**, 7509-7530,
765 (2022).

766 103 Saidaminov, M. I. *et al.* Suppression of atomic vacancies via incorporation of isovalent small
767 ions to increase the stability of halide perovskite solar cells in ambient air. *Nat. Energy* **3**,
768 648-654,(2018).

769 104 Deger, C., Tan, S., Houk, K. N., Yang, Y. & Yavuz, I. Lattice strain suppresses point defect
770 formation in halide perovskites. *Nano Research* **15**, 5746-5751,(2022).

771 105 Kim, G. *et al.* Impact of strain relaxation on performance of α -formamidinium lead iodide
772 perovskite solar cells. *Science* **370**, 108-112,(2020).

773 106 Lee, J.-H. *et al.* Resolving the Physical Origin of Octahedral Tilting in Halide Perovskites.
774 *Chemistry of Materials* **28**, 4259-4266,(2016).

775 107 Wang, L. *et al.* [PbX₆]⁴⁻ modulation and organic spacer construction for stable perovskite
776 solar cells. *Energ. Environ. Sci.* **15**, 4470-4510,(2022).

777 108 Shi, Y. & Chu, L. Dipole polymer-coated crystalline grains to endure temperature variations
778 of perovskite photovoltaics. *Matter* **6**, 1063-1065,(2023).

779 109 Luo, D., Su, R., Zhang, W., Gong, Q. & Zhu, R. Minimizing non-radiative recombination
780 losses in perovskite solar cells. *Nature Reviews Materials* **5**, 44-60,(2020).

781 110 Zhang, Y. *et al.* Improved fatigue behaviour of perovskite solar cells with an interfacial
782 starch–polyiodide buffer layer. *Nature Photonics* **17**, 1066-1073,(2023).

783 111 Teng, T. Y. *et al.* Electronically Manipulated Molecular Strategy Enabling Highly Efficient
784 Tin Perovskite Photovoltaics. *Angewandte Chemie* **136**, e202318133,(2024).

785 112 Dai, Z. *et al.* Dual-Interface-Reinforced Flexible Perovskite Solar Cells for Enhanced
786 Performance and Mechanical Reliability. *Advanced Materials* **34**, 2205301,(2022).

787 113 Zhang, C.-C. *et al.* Perovskite Films with Reduced Interfacial Strains via a Molecular-Level
788 Flexible Interlayer for Photovoltaic Application. *Advanced Materials* **32**, 2001479,(2020).

789 114 Kaltenbrunner, M. *et al.* Flexible high power-per-weight perovskite solar cells with chromium
790 oxide–metal contacts for improved stability in air. *Nature Materials* **14**, 1032-1039,(2015).

791 115 Domanski, K. *et al.* Not All That Glitters Is Gold: Metal-Migration-Induced Degradation in
792 Perovskite Solar Cells. *ACS Nano* **10**, 6306-6314,(2016).

793 116 Tress, W. *et al.* Performance of perovskite solar cells under simulated temperature-
794 illumination real-world operating conditions. *Nature Energy* **4**, 568-574,(2019).

795 117 Zhang, G. *et al.* Shellac protects perovskite solar cell modules under real-world conditions.
796 *Joule* **8**, 496-508,(2024).

797 118 Li, J. *et al.* Ink Design Enabling Slot-Die Coated Perovskite Solar Cells with >22% Power
798 Conversion Efficiency, Micro-Modules, and 1 Year of Outdoor Performance Evaluation.
799 *Advanced Energy Materials* **13**, 2203898-2203898,(2023).

800 119 Aydin, E. *et al.* Interplay between temperature and bandgap energies on the outdoor
801 performance of perovskite/silicon tandem solar cells. *Nature Energy* **5**, 851-859,(2020).

802 120 Xie, H. *et al.* Decoupling the effects of defects on efficiency and stability through
803 phosphonates in stable halide perovskite solar cells. *Joule* **5**, 1246-1266,(2021).

804 121 Babics, M. *et al.* One-year outdoor operation of monolithic perovskite/silicon tandem solar
805 cells. *Cell Reports Physical Science* **4**,(2023).

806 122 Liu, K., Wang, Z., Qu, S. & Ding, L. Stress and Strain in Perovskite/Silicon Tandem Solar
807 Cells. *Nano-Micro Letters* **15**, 59,(2023).

808 123 Dailey, M., Li, Y. & Printz, A. D. Residual Film Stresses in Perovskite Solar Cells: Origins,
809 Effects, and Mitigation Strategies. *ACS Omega* **6**, 30214-30223,(2021).

810 124 Sahli, F. *et al.* Fully textured monolithic perovskite/silicon tandem solar cells with 25.2%
811 power conversion efficiency. *Nature Materials* **17**, 820-826,(2018).

812 125 Sahli, F. *et al.* Improved Optics in Monolithic Perovskite/Silicon Tandem Solar Cells with a
813 Nanocrystalline Silicon Recombination Junction. *Advanced Energy Materials* **8**, 1701609,
814 (2018).

815 126 Chen, B. *et al.* Blade-Coated Perovskites on Textured Silicon for 26%-Efficient Monolithic
816 Perovskite/Silicon Tandem Solar Cells. *Joule* **4**, 850-864,(2020).

817 127 Jiang, J. *et al.* Synergistic strain engineering of perovskite single crystals for highly stable and
818 sensitive X-ray detectors with low-bias imaging and monitoring. *Nature Photonics* **16**, 575-
819 581,(2022).

820 128 Roß, M. *et al.* Co-Evaporated Formamidinium Lead Iodide Based Perovskites with 1000 h
821 Constant Stability for Fully Textured Monolithic Perovskite/Silicon Tandem Solar Cells.
822 *Advanced Energy Materials* **11**, 2101460,(2021).

823 129 Dupré, O., Vaillon, R. & Green, M. A. Physics of the temperature coefficients of solar cells.
824 *Solar Energy Materials and Solar Cells* **140**, 92-100,(2015).

825 130 Babics, M., Bristow, H., Pininti, A. R., Allen, T. G. & De Wolf, S. Temperature Coefficients
826 of Perovskite/Silicon Tandem Solar Cells. *ACS Energy Letters* **8**, 3013-3015,(2023).

827 131 Cheacharoen, R. *et al.* in *2018 IEEE 7th World Conference on Photovoltaic Energy
828 Conversion (WCPEC)* . 3498-3502.

829 132 Delmas, W. *et al.* Evaluation of Hybrid Perovskite Prototypes After 10-Month Space Flight
830 on the International Space Station. *Advanced Energy Materials* **13**, 2203920-2203920,(2023).

831 133 Tu, Y. *et al.* Perovskite Solar Cells for Space Applications: Progress and Challenges.
832 *Advanced Materials* **33**, 2006545,(2021).

833 134 Jošt, M. *et al.* Perovskite Solar Cells go Outdoors: Field Testing and Temperature Effects on
834 Energy Yield. *Advanced Energy Materials* **10**, 2000454-2000454,(2020).

835 135 Reese, M. O. *et al.* Consensus stability testing protocols for organic photovoltaic materials
836 and devices. *Solar Energy Materials and Solar Cells* **95**, 1253-1267,(2011).

837 136 Rombach, F. M., Haque, S. A. & Macdonald, T. J. Lessons learned from spiro-OMeTAD and
838 PTAA in perovskite solar cells. *Energy & Environmental Science* **14**, 5161-5190,(2021).

839 137 Cheacharoen, R. *et al.* Encapsulating perovskite solar cells to withstand damp heat and
840 thermal cycling. *Sustainable Energy & Fuels* **2**, 2398-2406,(2018).

841 138 Jiao, H. *et al.* Metal Halide Perovskite Solar Module Encapsulation Using Polyolefin
842 Elastomers: The Role of Morphology in Preventing Delamination. *PRX Energy* **3**, 023013,
843 (2024).

844 139 Gratia, P. *et al.* The Many Faces of Mixed Ion Perovskites: Unraveling and Understanding the
845 Crystallization Process. *ACS Energy Letters* **2**, 2686-2693,(2017).

846 140 Thind, A. S., Huang, X., Sun, J. & Mishra, R. First-Principles Prediction of a Stable
847 Hexagonal Phase of CH₃NH₃PbI₃. *Chemistry of Materials* **29**, 6003-6011,(2017).

848 141 Shao, S. *et al.* Efficient Perovskite Solar Cells over a Broad Temperature Window: The Role
849 of the Charge Carrier Extraction. *Advanced Energy Materials* **7**, 1701305-1701305,(2017).

850 142 Isikgor, F. H. *et al.* Molecular engineering of contact interfaces for high-performance
851 perovskite solar cells. *Nature Reviews Materials* **8**, 89-108,(2023).

852 143 Holzhey, P. & Saliba, M. A full overview of international standards assessing the long-term
853 stability of perovskite solar cells. *Journal of Materials Chemistry A* **6**, 21794-21808,(2018).

854

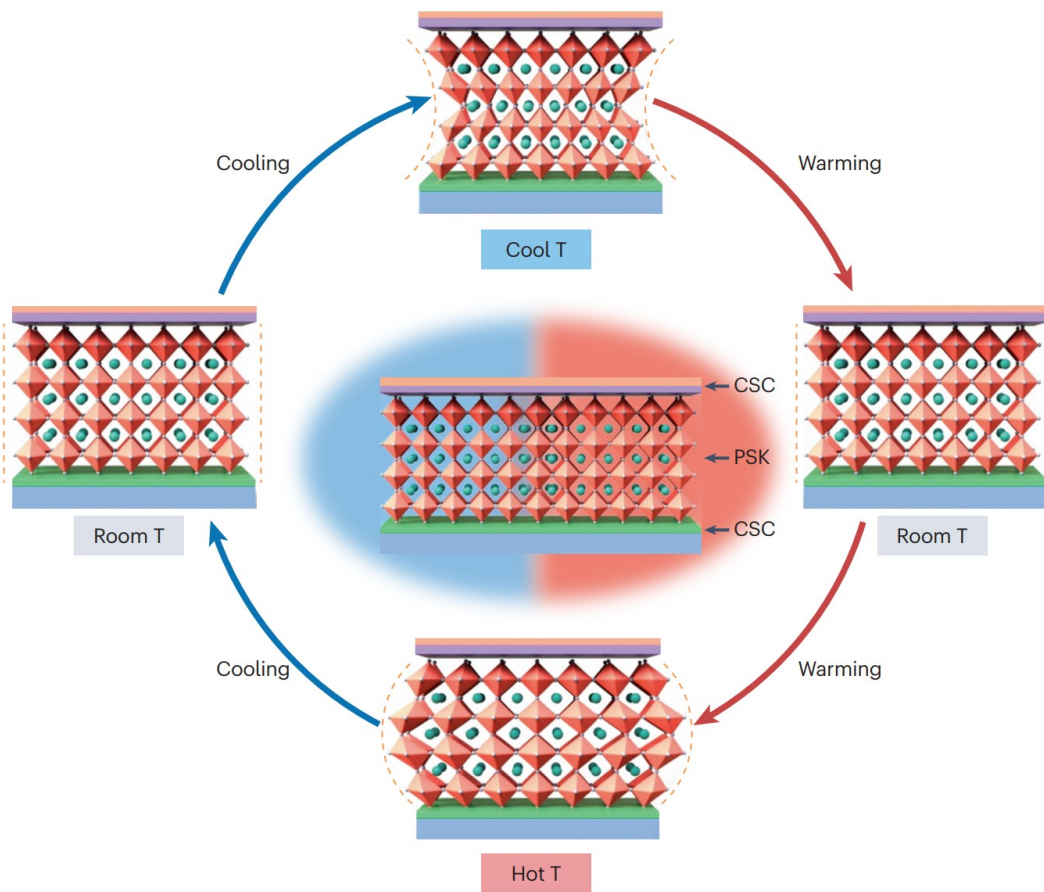
855 **Table 1 | Established ISOS protocols that account for the temperature cycling of perovskite**
856 **materials and devices¹⁹.**

Test ID	Light Source	Temperature	Rel. humidity	Environment/Set-up	Load
ISOS-T-1	None	RT to +65, +85 °C	Ambient	Hot plate/Oven	OC

ISOS-T-2		RT to +65, +85 °C	Ambient	Oven/env. chamber	OC
ISOS-T-3		-40 to +85 °C	< 55%	Env. chamber	OC
ISOS-LT-1		Linear or step ramping between room temp and +65 °C	Monitored, uncontrolled	Weather chamber	MPP or OC
ISOS-LT-2	Solar simulat or	Linear ramping between +5 to +65 °C	Monitored, controlled at 50% beyond +40 °C	Env. chamber with a sun simulator	MPP or OC
ISOS-LT-3		Linear ramping between -25 to +65 °C	Monitored, controlled at 50% beyond +40 °C	Env. chamber with sun simulator and freezing	MPP or OC

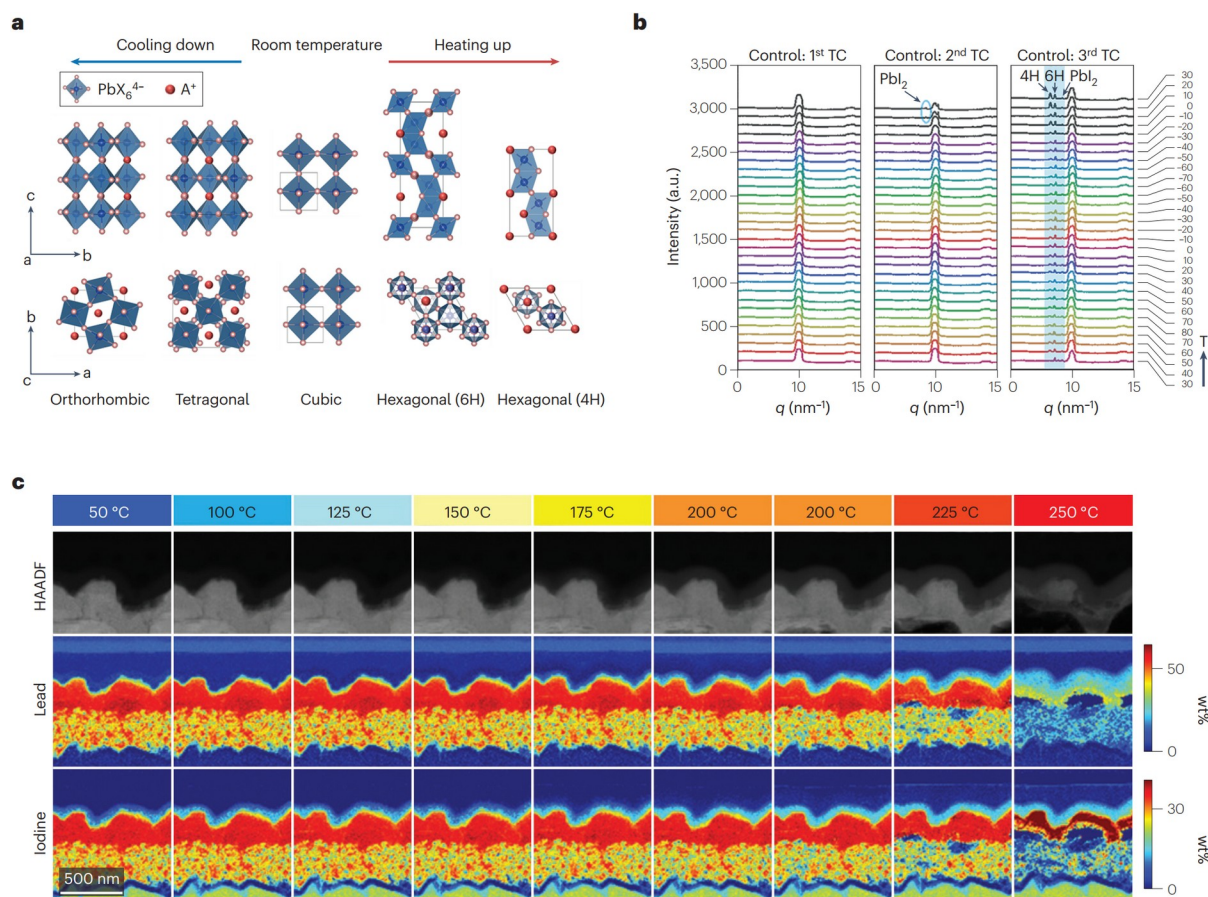
857

858



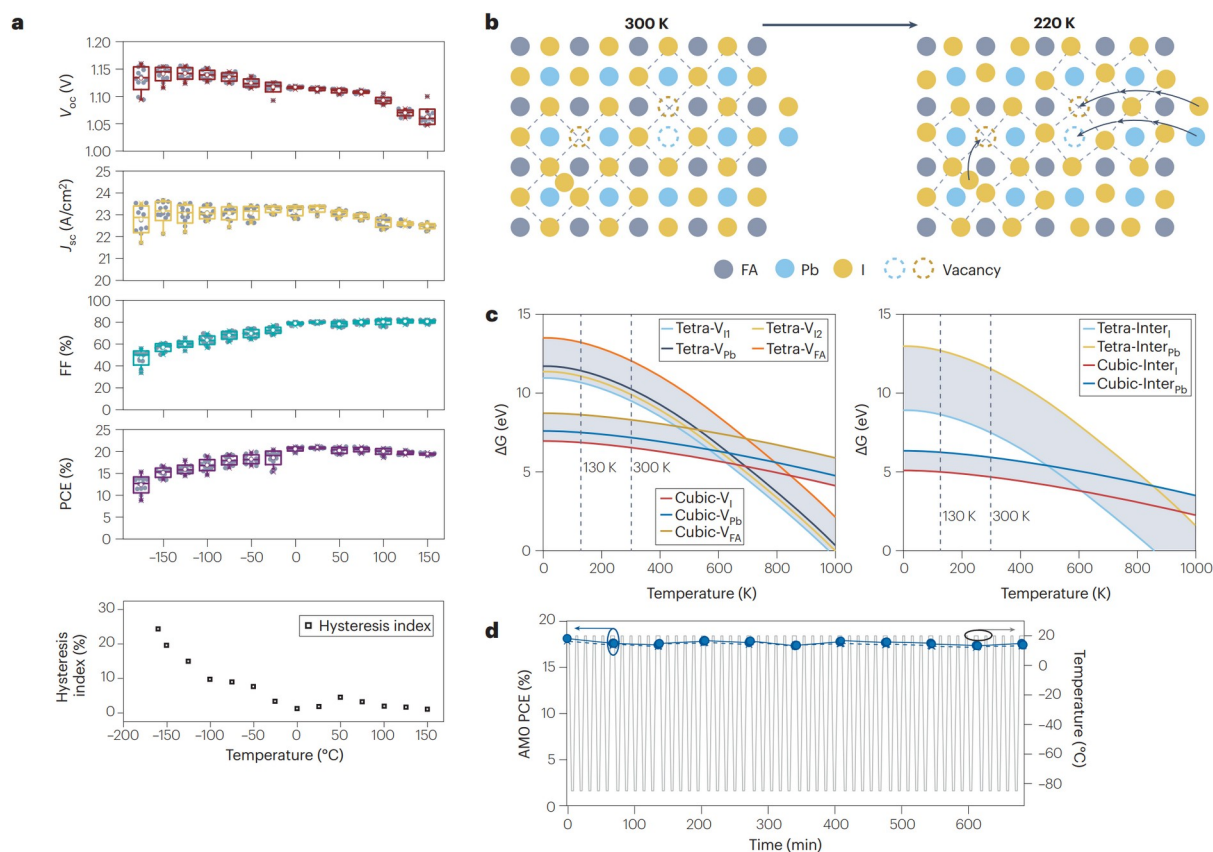
859

860 **Fig. 1 |The cycling temperature influence on perovskite structure in the device.** CSC denotes
 861 charge selective contact, PSK denotes perovskite, and T denotes temperature.



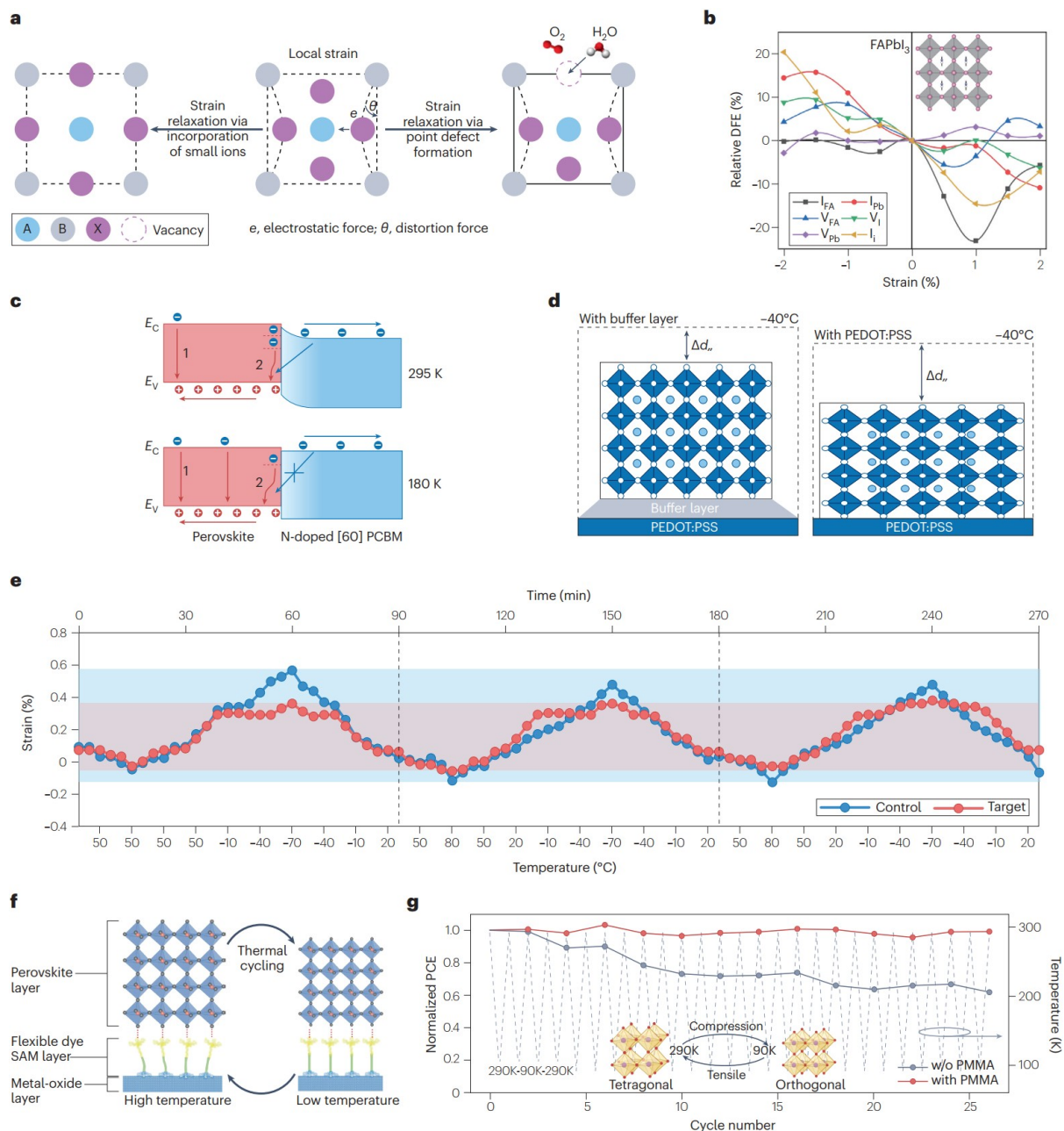
862

863 **Fig. 2 | Temperature influence on perovskite structure.** **a**, Crystal phases of FAMACs-based
 864 perovskites and evolution with temperature (perovskite structure evolution). **b**, Temperature-resolved
 865 grazing-incidence wide-angle X-ray scattering (GIWAXS) profiles for FAMACs-based perovskite
 866 film with highlighted PbI_2 peak arising (perovskite degradation and phase transition). **c**, High-angle
 867 annular dark-field (HAADF) images and energy-dispersive X-ray (EDX) elemental maps for iodine
 868 and lead for lamellae perovskite sample obtained after heating at different temperatures (interlayer
 869 material degradation). Figure **a** adapted with Permission from refs ^{139,140}. Figure **b** reprinted with
 870 Permission from ref.⁵⁷, 2023 AAAS. Figure **c** reprinted with Permission from ref.⁷¹, 2016 Springer
 871 Nature Limited.



872

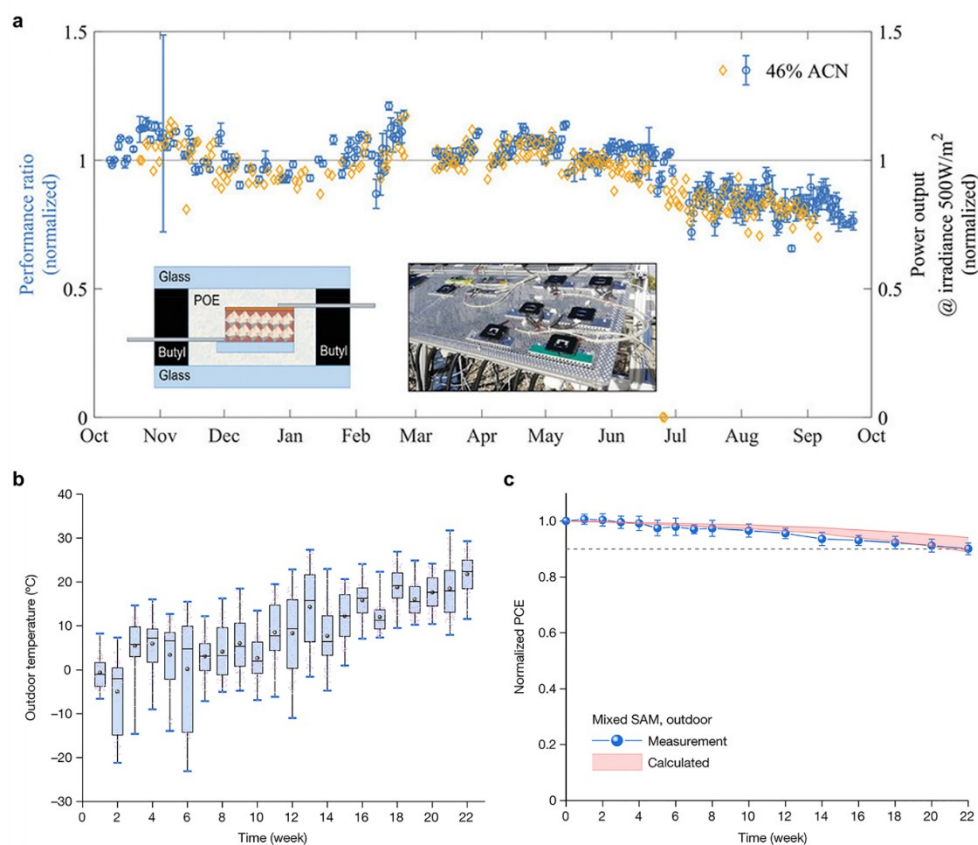
873 **Fig. 3 | Device performance parameters with temperature variation.** **a**, Statistical box charts of
 874 V_{OC} , J_{SC} , FF, PCE and HI distribution of PSCs at different temperatures (The temperature-induced
 875 changes in PCE are primarily driven by opposing trends in V_{OC} , with PCE following the same trend as
 876 FF and HI.). **b**, A schematic illustration for the self-elimination of intrinsic defects via phase transition
 877 (Reducing the temperature aids in the elimination of intrinsic point defects in perovskite materials). **c**,
 878 The dependence of ΔG for vacancy and interstitial defects on the temperature. (Lowering the
 879 temperature induces a cubic-to-tetragonal phase transition, increasing defect-formation energy.) **d**,
 880 Evolution of PCE of PSCs during 50 thermal cycling between +20 and $-80^{\circ}C$ at 10 mbar under
 881 constant AM0 illumination (blue symbols correspond to the PV parameters on the left, and the solid
 882 grey lines refer to the temperature on the right). (Perovskite devices have reversible performance
 883 behavior upon returning to room temperature) Figures **a**, **d** reprinted with Permission from ref.³², 2022
 884 Wiley. Figures **b** and **c** reprinted with Permission from ref.⁶⁴, 2020, Elsevier



885

886 **Fig. 4 | Strategies for enhancing photovoltaic performance under thermal cycling.** **a**, Schematic
 887 illustrating the local strain, which is decreased by forming point defects or by doping with small ions
 888 (Strain relaxation via ion incorporation and defect formation). **b**, Relationship between defect
 889 formation energy (DFE) and lattice strain (Defect formation energy control). **c**, Schematic diagram of
 890 charge extraction and recombination at the perovskite/N-doped PC₆₁BM interface at maximum power
 891 point at 295 (+21.85, top) and 180 K (-93.15 °C, bottom) (Temperature-induced interfacial charge
 892 transport). **d**, Schematic diagram of strain formation process and reduction of strain through buried
 893 interface modification with or without buffer layer between PEDOT:PSS and Sn perovskites (Buffer
 894 layer at the interface). **e**, The temperature-resolved lattice strain for control and target perovskites.
 895 (The temperature starts from room temperature, heating to +80 °C and then cooling to -60 °C. The

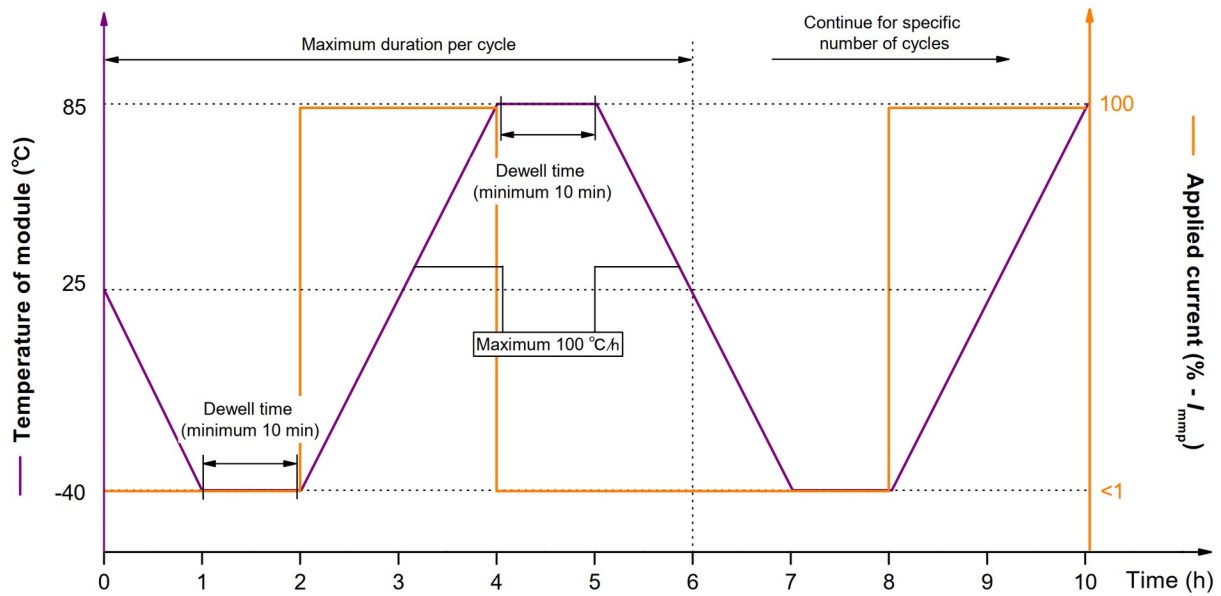
896 progress ends at room temperature. The time per complete cycle is 90 min.) (Ordered dipole structure
 897 polymer-coated perovskite crystals). **f**, Illustration of how flexible dye self-assembled monolayers
 898 (SAMs) alleviate compressive and tensile stresses in perovskite films going through a thermal cycling
 899 process (Interfacial flexible SAMs to release strain). **g**, Normalized temperature cycling test between
 900 290 (+16.85) and 90 K (-183.15 °C) for the PSCs with and without PMMA interlayer (Interlayer-
 901 regulated thermal cycling performance). Figure **a** reprinted with Permission from ref.¹⁰³. Figure **b**
 902 adapted with permission from ref.¹⁰⁴, 2022 Springer. Panel **c** adapted with Permission from ref.¹⁴¹, [CC](#)
 903 [BY 4.0](#). Panel **d** reprinted with Permission from ref.¹¹¹, 2024 Wiley. Panel **e** reprinted with Permission
 904 from ref.⁵⁷, 2023 AAAS. Figure **f** reprinted with Permission from ref.¹⁴², 2022 Springer Nature
 905 Limited. Figure **g** reprinted with Permission from ref.⁹³, 2023 Elsevier.



906

907 **Fig. 5 | PV performance under real-world diurnal cycles.** **a**, Time evolution of normalized
 908 performance ratio (averaged over three PSCs) and cell MPP tracking at a power of 500 W m^{-2} during
 909 the outdoor exposure (ISOS-O-2) for small area devices. The inserted photographs are the devices
 910 fixed outdoors in an open rack configuration and schematics of device encapsulation. **b**, Outdoor
 911 ambient temperature trend. **c**, Normalized PCE evolution of packaged devices under outdoor ageing
 912 conditions. The pink band shows the calculated trend. The error bars represent the standard deviations

913 from 14 individual packaged devices. Figure a reprinted with Permission from ref.¹¹⁸, 2023 Wiley.
914 Figures b to c reprinted with Permission from ref.⁵³, 2023 Springer Nature Limited.



915

916 **Fig. 6 | Graphic representation of the recommended thermal cycling profile.** During the heating
917 from -40 to $+80$ °C at a current of 10% of the maximum power current for CIGS, CdTe and
918 amorphous silicon. For crystalline silicon, it is 100%. The heating and cooling should not be lower
919 than 45 °C h^{-1} . Sketch of the accelerated ageing tests prescribed by IEC standards.

920